Materials Horizons

COMMUNICATION

Cite this: *Mater. Horiz.*, 2016, 3, 596

Received 26th July 2016,
Accepted 13th September 2016

DOI: 10.1039/c6mh00270f

www.rsc.li/materials-horizons

Hierarchical self-assembly of a bulk metamaterial enables isotropic magnetic permeability at optical frequencies†

S. Gomez-Graña,[a] A. Le Beulze,[a] M. Treguer-Delapierre,[a] S. Mornet,[a] E. Duguet,[a] E. Grana,[b] E. Cloutet,[b] G. Hadziioannou,[b] J. Leng,[c] J.-B. Salmon,[c] V. G. Kravets,[d] A. N. Grigorenko,[d] N. A. Peyyety,[e] V. Ponsinet,[e] P. Richetti,[e] A. Baron,[e] D. Torrent[e] and P. Barois*[e]

Raspberry-like magnetic nanoclusters are synthesized and subsequently self-assembled to form a bulk metamaterial exhibiting strong isotropic optical magnetism in visible light. The magnetic response of the nanoclusters (metamolecules) and of the final assembled material are measured by independent optical experiments. The validity of the effective permeability parameter is probed by spectroscopic ellipsometry at variable incidence. Numerical simulations confirm the measurements.

Conceptual insights

Controlling the magnetic permeability μ of artificial materials is expected to offer an unprecedented control of the flow of light in optical devices. Unfortunately, the magnetic response of natural materials is negligible at optical frequencies. A rational design of nano-composites enables here the operational extension of the concept of magnetic permeability to visible light. Up to now, artificial optical magnetism has been observed in anisotropic structures thinner than the wavelength of light as a non-local effect which is too complex to be described by an effective magnetic permeability tensor, hence precluding the use of the usual laws of reflection and refraction. In contrast, the reflection of light by our novel magnetic metamaterial obeys the classical laws of optics at variable incidence. This fundamental approach, based on the precise control of the structural symmetry of the material at all steps of a hierarchical self-assembly process, provides strict guidelines for the design of magnetic materials described by a valid permeability parameter. This strategy can be readily extended to the future generation of low-loss, all-dielectric metamaterials, hence renewing the interest for extraordinary applications of metamaterials based on non natural values of μ.

The ability to control independently the values of the dielectric permittivity (ε) and of the magnetic permeability (μ) of optical materials would open extraordinary applications that have been abundantly discussed in the field of metamaterials. The perfect lens, based on a hypothetical negative index material resulting from simultaneous negative values of ε and μ, and the invisibility cloak, based on the concept of transformation optics implying the realization of well controlled gradients of ε and μ were seminal proposals of the field.[1,2] Applications of transformation optics are foreseen not just in cloaking, which consists of bending light around an obstacle to make it invisible, but also in light concentrators, for the generation of intense fields for sensing or nonlinear optics, or for optical impedance matching, enabling a more efficient collection of light in optical devices.[3,4] Controlling μ is notoriously difficult since the magnetic susceptibility of natural materials is negligible in visible light.[5] Consequently, the generation of optical magnetism has been intensively searched in artificial nanocomposites, generally designed so as to develop loops of intense induced currents upon illumination by a light wave.[6–11] While the use of noble metals has unveiled the fundamental limitations due to optical losses associated with plasmonic resonances, the perspective of future all-dielectric optical devices based on Mie resonances restores the interest of understanding the light–matter interaction leading to artificial magnetism.[12,13] The self-assembly method described here is indeed applicable to the next generation of all-dielectric metamaterials.

All the appealing properties of magnetic metamaterials cited above rest upon the implicit assumption that the magnetic permeability μ maintains in artificial composites its familiar meaning based on the introduction in Maxwell's equations of the auxiliary fields $\mathbf{H} = \mathbf{B}/\mu_0\mu$ and $\mathbf{D} = \varepsilon_0\varepsilon\mathbf{E}$ deriving from the alleged structure of the induced current density $\mathbf{J} = \nabla \times \mathbf{M} - i\omega\varepsilon_0\varepsilon\mathbf{E}$ in which $\mathbf{M}$ identifies with a local density of magnetization and the time dependence is assumed to be $\exp(-i\omega t)$. This is unfortunately not true in general since the space and time derivatives of the induced currents cannot be separated. A more rigorous approach consists in using a non local dielectric tensor $\varepsilon_{ij}(\omega,\mathbf{k})$ accounting for the wave vector $\mathbf{k}$

[a] *University of Bordeaux, CNRS, ICMCB, UPR 9048, 33600 Pessac, France*
[b] *University of Bordeaux, CNRS, LCPO, UMR 5629, 33615 Pessac, France*
[c] *University of Bordeaux, CNRS, Solvay, LOF, UMR 5258, 33608 Pessac, France*
[d] *School of Physics and Astronomy, University of Manchester, Manchester, M13 9PL, UK*
[e] *University of Bordeaux, CNRS, CRPP, UPR 8641, 33600 Pessac, France. E-mail: barois@crpp-bordeaux.cnrs.fr*

† Electronic supplementary information (ESI) available. See DOI: 10.1039/c6mh00270f

dependence of the electromagnetic response of the material, referred to as spatial dispersion.[14,15] In the case of weak spatial dispersion, the frequency and wave vector dependences can be separated in a power-series expansion $\varepsilon_{ij}(\omega,\mathbf{k}) = \varepsilon_{ij}(\omega) + \beta_{ijl}(\omega)k_l + \gamma_{ijlm}(\omega)k_l k_m$. For achiral systems, $\beta_{ijl}(w) = 0$ and the artificial magnetism is depicted by the fourth rank tensor $\gamma_{ijlm}(\omega)$, making it obvious that the usual second rank permeability tensor μ_{ij} will not suffice to describe the optical properties. The number of independent components of a fourth rank tensor actually ranges from 36 in a triclinic system to 4 in a cubic symmetry and reduces to 2 in an isotropic structure with C_∞ continuous spherical symmetry.[14]

For a second rank tensor, the number of independent elements is respectively 6, 1 and 1. Consequently, any attempt to describe the artificial optical magnetism by the sole permeability tensor μ_{ij} amounts to neglecting a set of parameters which is prohibitively large in systems of low symmetry, but which interestingly reduces to a single component in isotropic systems, which thus appear as the best candidates to enable an operational permeability approximation. Up to now, the observation of strong artificial magnetism at frequencies of visible or near-infrared light has been reported in several types of planar plasmonic nanostructures which are essentially two-dimensional and highly anisotropic.[7–11] For example, the inadequacy of the permeability tensor to describe the strong artificial magnetism observed in fishnet devices of tetragonal symmetry was discussed in ref. 16.

The material described in the present work is built on a different rational approach designed so as to produce a nanostructure with a perfect spherical symmetry in order to check the validity of a magnetic permeability parameter, under the most favorable symmetry conditions. The locality of the isotropic structure is directly demonstrated by the absence of angular dependence of the extracted optical parameters ε and μ. Our bottom-up strategy consists in a hierarchical self assembly process starting with the chemical synthesis of spherical magnetic nanoclusters (MNC) followed by the self-assembly of these meta-atoms in a random close packing. The ''Raspberry-like'' structure of the MNCs consists of a set of metallic nanoparticles evenly distributed at the surface of a core dielectric sphere (Fig. 1a–c) which behave like a resistor–inductor–capacitor (RLC) nanocircuit. The artificial magnetic response is generated by resonant loops of plasmonic currents induced by the light wave.[17] The spherical morphology proposed by Simovski and Tretyakov is chosen so as to forbid bi-anisotropic effects and maximize artificial magnetism γ among all the second-order spatial dispersion effects.[18]

The fabrication of the metamaterial starts with the synthesis of the meta-atoms according to the Simovski–Tretyakov model (Fig. 1a–c).[18] The large scale production of MNCs of well controlled morphology is critical for the fabrication of a homogeneous bulk material of macroscopic size. Non specific electrostatic forces as well as specific protein or DNA mediated interactions have been used to self-assemble particles at the nano scale.[19–25] In the present work, large amounts of MNCs are synthesized in aqueous dispersions by electrostatic self-assembly

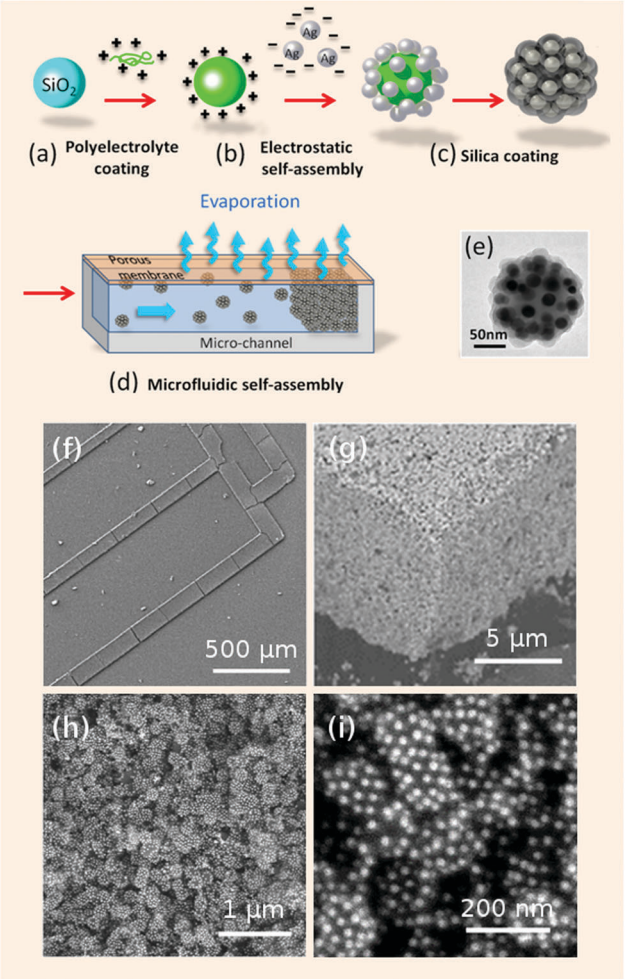

Fig. 1 (a–d) Sketch of the hierarchical self-assembly process. Silica nanoparticles coated by a polycation (a) self-assemble with negatively charged silver nanoparticles (b) to form raspberry-like meta-molecules similar to the Simovski–Tretyakov model of magnetic nanocluster (MNC).[18] An outer silica layer is grown (c) to secure the nanostructure. The MNCs are subsequently assembled in a microfluidic evaporator (d) to form a bulk metamaterial. (e) Transmission Electron Microscopy micrograph of a real MNC. (f–i) High-Resolution Scanning Electron Microscopy images of the resulting material at different scales, showing the neat geometrical features of the dense solid made of randomly packed MNCs.

of positively charged silica cores of diameter 96 ± 3 nm and negatively charged silver satellites of diameter 25 ± 2 nm. A thin layer (5 nm) of silica is grown on the surface of the clusters to secure their morphology and improve their colloidal stability (Fig. 1e). We then formulate the bulk metamaterial in a microfluidic device by slow evaporation of the solvent across a thin polymer membrane (Fig. 1d and f).[26–28] The final 3D-material is a solid phase made of densely packed MNCs with a volume fraction estimated to be 60(±5)%, which is consistent with a random close packing of spheres. Fig. 1f reveals the excellent definition of the outer shape of the final 3D material, perfectly replicating the micro-channel template with a surface roughness set by the size of the MNCs.

It is essential to check the presence and measure the strength of the magnetic response of the MNCs prior to assembling them.

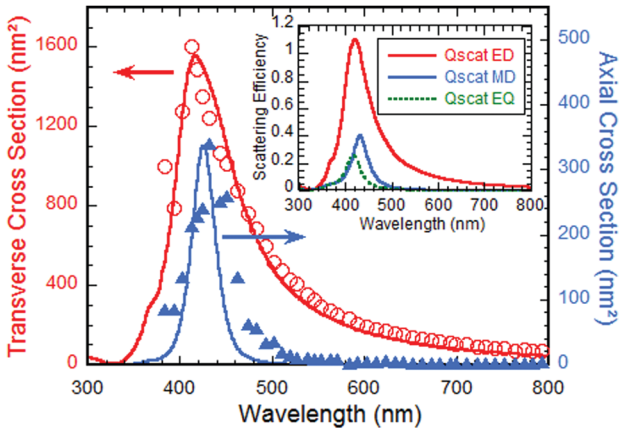

Fig. 2 Scattering cross-sections measured at 90° scattering angle on a dispersion of magnetic nanoclusters (MNCs) for two different output polarizations. The transverse (circles) and axial (triangles) signals are dominated respectively by the scattering of the electric dipole (ED) and the added contributions of the magnetic dipole (MD) and electric quadrupole (EQ).[29] Solid lines are T-Matrix numerical simulations of a MNC constructed along the model of Fig. 1a–c with 22 silver satellites coated with silica. Inset shows scattering efficiencies of the dipolar and quadrupolar modes. The efficiency of the dipolar magnetic scattering is found 2.5 times higher than the value measured on similar MNCs made with gold satellites.[21]

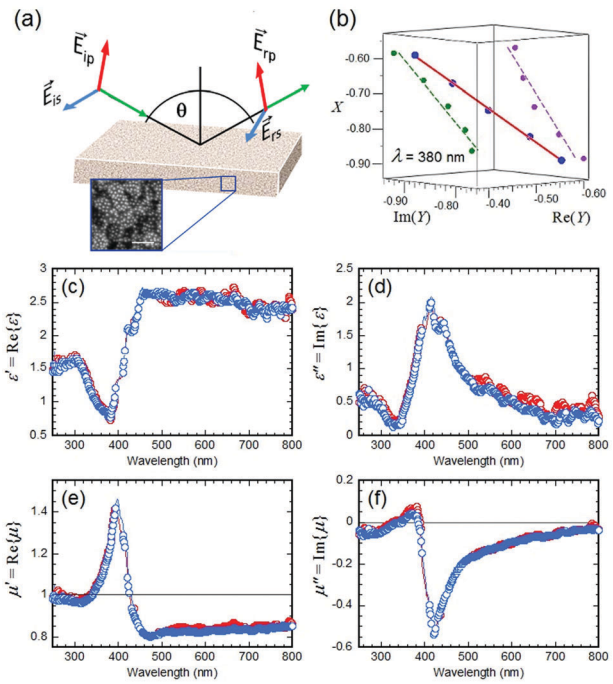

Fig. 3 (a) Geometry of the ellipsometric experiment. (b) Illustration of the linear relationship $Y = AX + B$ (see text) at a particular wavelength λ = 380 nm (solid line). Dashed lines show the projections of the linear form onto the planes (X, Re(Y)) purple and (X, Im(Y)) green. (c, d) and (e, f) Real and imaginary part of the permittivity ε and of the permeability μ respectively. Two different colours correspond to data collected by spectroscopic ellipsometry at two different positions in the sample. Solid lines display all data whereas the circles denote those points for which the correlation coefficient of the linear regression (eqn (1)) is higher than 0.95, indicating that the optical parameters ε and μ do not depend on the angle of incidence.

Following a method described in ref. 21 and 29, the scattering properties of dilute suspensions of MNCs were studied across the whole visible spectrum (400–800 nm) by a polarization resolved light scattering setup. The transverse and axial signals collected at 90° scattering angle along polarizations respectively perpendicular and parallel to the scattering plane are displayed in Fig. 2. In order to interpret the experimental signals, the scattering cross sections of a single MNC were computed by a T-Matrix code.[30] The electromagnetic response increases with the size and number of satellites.[31] An excellent agreement with experimental data is obtained for an average number of 22 silver satellites, consistent with real images obtained by transmission electron microscopy (Fig. 1e). The numerical T-Matrix expansion over vector spherical harmonics yields the series of scattering coefficients of a single MNC a_n and b_n.[30,32] It reveals that the scattering results from three dominant contributions, namely the radiation of the electric dipole (a_1) collected along the transverse direction and the combined radiation of the magnetic dipole (b_1) and of the electric quadrupole (a_2) both contributing to the axial signal (Fig. 2).[29] The axial to transverse signal reaches a record value of 0.28 at a wavelength of 430 nm, significantly higher than the highest reported level.[21,23] The scattering efficiency of the magnetic dipole reaches 0.4, 2.5 times higher than the value measured from MNCs of similar morphology but made with gold satellites.[21] We conclude from this light scattering study that the Simovski–Tretyakov MNCs made of silver satellites exhibit the expected magnetic response at unprecedented level, in perfect agreement with numerical simulations.

We resort to variable angle spectroscopic ellipsometry to retrieve the effective electromagnetic parameters of the formulated metamaterial. We measure the complex ellipsometric ratio $\rho = r_p/r_s$ where r_p and r_s are the amplitude reflection coefficients for light polarization parallel (p), and perpendicular (s) to the plane of incidence (Fig. 3a). The data analysis is based on two key features: (i) the sample is thicker than the absorption length of the material and behaves as a semi-infinite material and (ii) the Fresnel formulae are written as functions of the impedance $Z = (\mu/\varepsilon)^{1/2}$ to account for variable permeability. A simple analytic relationship between the ellipsometric ratio ρ and the material parameters ε and μ follows:

$$\left(\frac{1-\rho}{1+\rho}\right)^2 \frac{\sin^4\theta}{\cos^2\theta} = -A\sin^2\theta + B \qquad (1)$$

with

$$A = \left(\frac{\mu-\varepsilon}{1-\mu\varepsilon}\right)^2, \quad B = \varepsilon\mu\left(\frac{\mu-\varepsilon}{1-\mu\varepsilon}\right)^2$$

where θ is the angle of incidence in the ambient air medium.

Eqn (1) has a linear form $Y = AX + B$ that enables the extraction of the unknown coefficients A and B for each wavelength from a linear regression of the experimental quantities X and Y measured on a set of five different angles separated by 5° from 50 to 70° (Fig. 3b). Inverting the pair of quadratic equations for A and B yields a set of 4 solutions (ε,μ) among which the physical ones are

selected so as to satisfy the physical constraints that the imaginary part k of the refractive index and the real part Z' of the optical impedance Z should be positive.

The physical solutions are displayed for two different positions in the sample in Fig. 3c–f. Both effective parameters ε and μ exhibit a resonant behavior centered at $\lambda \cong 420$ nm. The magnetic permeability deviates notably from the natural value $\mu = 1 + 0i$ with a real part μ' ranging from 0.8 to 1.45 and a negative imaginary part μ''. These variations reveal a real part of the magnetic susceptibility $\chi_m = \mu - 1$ reaching a negative peak value of approximately -0.2 at $\lambda = 460$ nm, three orders of magnitude stronger than the record natural static diamagnetic susceptibility of graphite, and a positive peak value of +0.45 at $\lambda = 400$ nm, opposite to the classical negative sign of diamagnetism.[35] The goodness of the linear fit to eqn (1) throughout the wavelength range is evidenced in Fig. 3c–f by symbols denoting those data points for which the Pearson correlation coefficient of the linear regression is larger than 0.95.[36] It demonstrates that neither ε nor μ depend on the direction θ of the incident wave vector **K** in the experimental range. The imaginary part of the effective refractive index $N = n + ik = \sqrt{\varepsilon\mu}$ enables to check the consistency of the semi-infinite condition. The propagation length $\lambda/4\pi k$ is indeed shorter than the thickness of the sample for wavelengths below 650 nm. For longer wavelengths in the non dispersive region, lower values of k are comparable to the experimental noise which may result in some experimental uncertainty (see Fig. S7 in ESI†).

Although negative values of the imaginary part μ'' of the magnetic permeability were already reported in theoretical and numerical studies of metamaterials, it is an unusual result that deserves some comment.[33,34] The whole electromagnetic response of the MNCs arises from plasmonic resonant modes generated by a unique driving force, namely the electric field of the light wave. The (ε,μ) approach is an approximation that formally splits the unique spatially dispersive electric response into a pair of more familiar electric-like and magnetic-like responses, the latter deriving from second order spatial derivatives of the electric field. Physical laws impose that the sum of these two inseparable processes must be dissipative. Propagation and reflection at an interface cause no problem as long as the imaginary part k of the refractive index and the real part Z' of the impedance are positive. However, one should not overlook the physical origin of the electromagnetic response of the MNC, which if fundamentally non-local and due to the inhomogeneous electric field. Non-locality means that the response in one point of the MNC depends on the polarizability in neighbouring points, up to some finite distance ξ which cannot be shorter than a MNC diameter. Indeed, the strong electric polarization of each satellite results from the presence of other satellites to form the resonant RLC nanocircuit. Consequently, it makes no sense to consider the sole magnetic polarization at scales shorter than ξ. The electric field is indeed always present at scale ξ and the sum of the electric and magnetic contributions over a volume ξ^3 is always dissipative. We shall see below that ξ can be estimated as comparable to a MNC diameter.

The major result of this ellipsometric study is therefore the demonstration that the metamaterial exhibits giant effective isotropic diamagnetism without any observable effect of spatial dispersion. To the best of our knowledge, this is the first time that the optical reflection properties of a bulk homogeneous material are correctly described at all angles of incidence by a unique non-natural permeability parameter μ at visible light frequencies.

Having measured the magnetic response of the MNC building blocks in a solvent by light scattering and the effective magnetic permeability of the bulk material by variable angle spectroscopic ellipsometry, the consistency of these two independent studies can be checked by numerical simulations.

The numerical expansion over vector spherical harmonics which yields the scattering coefficients of a single MNC a_n and b_n enables the modeling of the self-assembled material by the finite-element method.[30,32] Owing to the complexity of the meta-atom, a direct simulation is however very demanding in computational time. The physics of the problem can still be captured while greatly reducing the computational load by replacing the MNC (made of 22 silica-capped silver spheres plus one silica core) with a single fictitious homogeneous sphere (HS) with effective parameters $(\varepsilon_{HS}, \mu_{HS})$ chosen so as to produce the same dipolar scattering as the MNC.[21] Mie theory provides exact expressions for the scattering coefficients a_n and b_n of the homogeneous sphere. Forcing equivalent scattering properties for the MNC and the HS yields a set of $2n$ equations $a_n(\text{MNC}) = a_n(\text{HS})$ and $b_n(\text{MNC}) = b_n(\text{HS})$ which can only be satisfied at dipolar order $n = 1$ for two unknown functions $(\varepsilon_{HS}, \mu_{HS})$. The solutions $\varepsilon_{HS}(\lambda)$ and $\mu_{HS}(\lambda)$ are computed numerically and displayed in Fig. 4a and b. Fig. 4c shows that the dipolar scattering coefficients ED and MD of the MNC are perfectly reproduced by the HS, but not the quadrupolar terms EQ. The erroneous EQ contribution of the HS can be rejected to lower wavelength, out of the experimental range, by reducing the radius of the HS (Fig. 4c). Replacing the MNC by a HS is hence an approximation that preserves the two strongest components of the scattered field with dipolar symmetry, but neglects the EQ component. We may then expect some limited discrepancy in the range 380–440 nm where the EQ mode of the MNC is present. The field map shown in Fig. 4d illustrates the magnetic dipolar response of the HS at the magnetic resonance.

The negative imaginary part of the magnetic permeability of the HS again deserves more comment. The introduction of the HS simplifies the computing problem but overlooks the non-local nature of the electromagnetic response of the MNC. As stated before, the response of the MNC, and therefore of the HS, should not be considered in a local framework, but as a whole. Fig. 4d shows that the electric field is present in the volume of the HS, even at the magnetic resonance. The energy balance within the HS is always dissipative: the dissipation associated with the electric component is always larger than the gain associated with the magnetic component (see ESI†). The accuracy of the numerical simulation reported below suggests that the non-locality range ξ does not extend beyond the size of

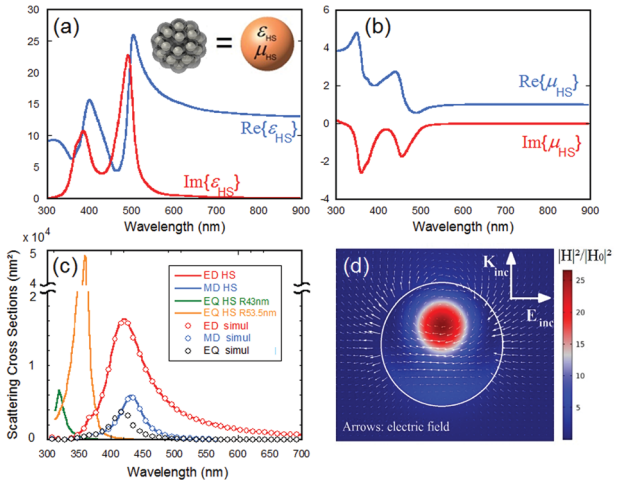

Fig. 4 (a and b) Spectral variations of the real and imaginary parts of the permittivity and of the permeability of the homogeneous sphere (HS) of radius R = 43 nm. (c) Scattering cross sections computed for the MNC (symbols) and for equivalent homogeneous spheres HS of two different radii R = 43 nm and R = 53.5 nm by the Mie theory (lines). The electric (ED) and magnetic (MD) dipolar scattering are rigorously identical for the three objects. The electric quadrupolar scattering (EQ) of the MNCs (black circles) is not reproduced by the HS of equivalent radius R = 53.5 nm (orange line). A smaller radius (R = 43 nm, green line) reduces the EQ scattering of the HS and pushes it towards lower wavelengths so that it does not contribute in the experimental range 380–800 nm. (d) Map of the squared magnetic field (color scale) and electric field (arrows) within the HS showing that the effective particle acts as a magnetic dipole at the magnetic resonance λ = 420 nm.

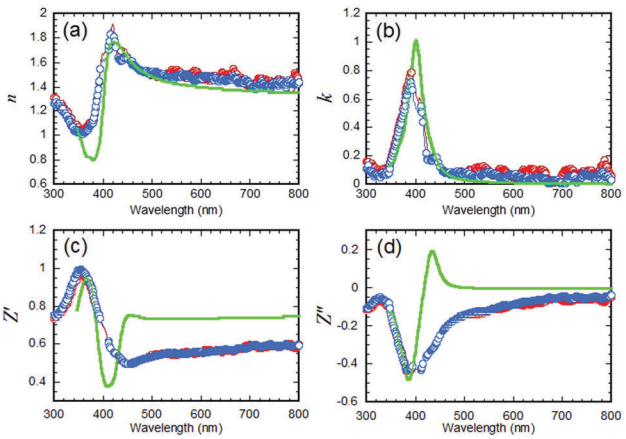

Fig. 5 Real and imaginary part of the refractive index (a and b) and of the optical impedance (c and d) of the metamaterial. Symbols and solid lines in blue and red correspond to the experimental data from spectroscopic ellipsometry shown in Fig. 3. The green line is a finite element numerical simulation of the optical properties of a cubic lattice homogeneous sphere (HS) shown in Fig. 4a and b.

a single MNC, hence confirming the situation of weak spatial dispersion.

Finally, we simulate a three dimensional arrangement of HSs on a simple cubic lattice to compute the response of a sample of assembled MNCs at normal incidence. The lattice parameter is set equal to the distance between closest neighbors in the compact arrangement (107 nm) in order to reproduce the pair interaction between nearest neighbours with a filling fraction of MNCs of 52%, which is close to the experimental estimate of 60%. There is no adjustable parameter. We use the finite element based commercial software COMSOL Multiphysics to compute the reflectance and transmittance coefficients under normal incidence, from which we deduce the spectral variations of the effective refractive index $N = n + ik$ and effective impedance $Z = Z' + iZ''$ of the metamaterial.[37] Fig. 5 compares the retrieved parameters to the experimental values extracted by variable angle spectroscopic ellipsometry. The numerical and experimental values of the four functions n, k, Z' and Z'' display very similar spectral variations. Moreover, the quantitative agreement is remarkably good for the refractive index (Fig. 5a and b). The full consistency between the values of the effective optical parameters obtained on the one hand with the normal angle retrieval method and scattering simulations and on the other hand by variable angle measurements further strengthens our claim that the bulk metamaterial fabricated in this work indeed satisfies the criterion of effective locality.[38]

Conclusions

Through a rational bottom-up multidisciplinary approach combining nano-chemistry, colloidal physics, spectroscopic ellipsometry, light scattering and numerical simulations, we created the first nanostructured metamaterial exhibiting at visible light frequencies a strong isotropic artificial optical magnetism which is correctly depicted by a valid magnetic permeability function μ. This result provides a higher relevance to the abundant literature describing extraordinary properties of metamaterials based on the control of the μ. Artificial magnetism, which arises from second order spatial dispersion, is by essence a non-local effect. The spatial disorder of the final material, inherent in self-assembly techniques, warrants the continuous spherical symmetry of the nanostructure, which we identify as a *conditio sine qua non* to minimize the non-locality phenomenon. We take advantage of the strong absorption associated with the plasmonic resonances to study our materials in the optically simple regime of a semi infinite medium. Losses are however not welcome and dielectric nanoresonators will undoubtedly serve as better candidates than plasmonic systems for future applications. This work should for example stimulate research for the synthesis of silicon nanospheres of well controlled size, which are not yet available in large amounts.[12,13] Whatever is the nature of the spherical meta-atom, this work paves the way to the large scale production of magnetic metamaterials of arbitrary shape and size, as required for future optical hardware.

Acknowledgements

This work was supported by the LabEx AMADEus (ANR-10-LABX-42) in the framework of IdEx Bordeaux (ANR-10-IDEX-03-02), France. The authors thank M. Malekovic for the synthesis of the silver satellites and Prof. C. Simovski for enlightening discussions about optical magnetism. EG, EC and GH acknowledge

financial support from the Industrial Chair (Arkema/ANR) within grant agreement number AC-2013-365.

References

1 J. B. Pendry, *Phys. Rev. Lett.*, 2000, **85**, 3966.
2 J. B. Pendry, D. Schurig and D. R. Smith, *Science*, 2006, **312**, 1780.
3 U. Leonhardt, *Science*, 2006, **12**, 1777.
4 V. M. Shalaev, *Science*, 2008, **322**, 384.
5 L. D. Landau and E. M. Lifshitz, *Electrodynamics of Continuous Media*, Pergamon Press, Oxford, 1960.
6 C. M. Soukoulis and M. Wegener, *Nat. Photonics*, 2011, **5**, 523.
7 A. N. Grigorenko, A. M. Geim, H. F. Gleeson, Y. Zhang, A. A. Firsov, I. Y. Khrushchev and J. Petrovic, *Nature*, 2005, **438**, 335.
8 S. Linden, C. Enkrich, M. Wegener, J. Zhou, T. Koschny and C. M. Soukoulis, *Science*, 2004, **306**, 1351.
9 J. Zhou, L. Zhang, G. Tuttle, Th. Koscny and C. M. Soukoulis, *Phys. Rev. B: Condens. Matter Mater. Phys.*, 2006, **73**, 041101(R).
10 G. Dolling, M. Wegener, C. M. Soukoulis and S. Linden, *Opt. Lett.*, 2007, **32**, 53.
11 T. Xu, A. Agrawal, M. Abashin, K. J. Chau and H. J. Lezec, *Nature*, 2013, **497**, 470.
12 S. Jahani and Z. Jacob, *Nat. Nanotechnol.*, 2016, **11**, 23.
13 A. B. Evlyukhin, S. M. Novikov, U. Zywietz, R. L. Eriksen, C. Reinhardt, S. I. Bozhevolnyi and B. N. Chichkov, *Nano Lett.*, 2012, **12**, 3749.
14 V. M. Agranovich and V. L. Ginzburg, in *Crystal Optics with Spatial Dispersion, and Excitons*, ed. M. Cardona, P. Fulde and H. J. Queisser, Springer-Verlag, Berlin, Heidelberg, 1984, vol. 42.
15 V. M. Agranovich and Y. N. Gartstein, *Phys.-Usp.*, 2006, **49**, 1029.
16 C. Menzel, T. Paul, C. Rockstuhl, T. Pertsch, S. Tretyakov and F. Lederer, *Phys. Rev. B: Condens. Matter Mater. Phys.*, 2010, **81**, 035320.
17 A. Alù, A. Salandrino and N. Engheta, *Opt. Express*, 2006, **14**, 1557.
18 C. R. Simovski and S. A. Tretyakov, *Phys. Rev. B: Condens. Matter Mater. Phys.*, 2009, **79**, 045111.
19 S. Mühlig, A. Cunningham, S. Scheeler, C. Pacholski, T. Bürgi, C. Rockstuhl and F. Lederer, *ACS Nano*, 2011, **5**, 6586.
20 H. Ghosh and T. Bürgi, *J. Phys. Chem. C*, 2013, **117**, 26652.
21 V. Ponsinet, P. Barois, S. M. Gali, P. Richetti, J. B. Salmon, A. Vallecchi, M. Albani, A. Le Beulze, S. Gomez-Grana, E. Duguet, S. Mornet and M. Treguer-Delapierre, *Phys. Rev. B: Condens. Matter Mater. Phys.*, 2015, **92**, 220414(R).
22 Z. Qian, S. P. Hastings, C. Li, B. Edward, C. K. McGinn, N. Engheta, Z. Fakhraai and S. J. Park, *ACS Nano*, 2015, **9**, 1263.
23 S. N. Sheikholeslami, H. Alaeian, A. L. Koh and J. A. Dionne, *Nano Lett.*, 2013, **13**, 4137.
24 Y. Zheng, T. Thai, P. Reineck, L. Qiu, Y. Guo and U. Bach, *Adv. Funct. Mater.*, 2013, **23**, 1519.
25 R. P. M. Höller, M. Dulle, S. Thomä, M. Mayer, A. M. Steiner, S. Förster, A. Fery, C. Kuttner and M. Chanana, *ACS Nano*, 2016, **10**, 5740.
26 J. Leng, B. Lonetti, P. Tabeling, M. Joanicot and A. Ajdari, *Phys. Rev. Lett.*, 2006, **96**, 084503.
27 J. Angly, A. Iazzolino, J. B. Salmon, J. Leng, S. P. Chandran, V. Ponsinet, A. Desert, A. Le Beulze, S. Mornet, M. Treguer-Delapierre and M. A. Correa-Duarte, *ACS Nano*, 2013, **7**, 6465.
28 S. Gómez-Grana, C. Fernandez-Lopez, L. Polavarapu, J. B. Salmon, J. Leng, I. Pastoriza-Santos and J. Perez-Juste, *Chem. Mater.*, 2015, **27**, 8310.
29 N. L. Sharma, *Phys. Rev. Lett.*, 2007, **98**, 217402.
30 D. W. Mackowski and M. I. Mishchenko, *J. Opt. Soc. Am. A*, 1996, **13**, 2266, http://www.eng.auburn.edu/users/dmckwski/scatcodes/.
31 A. Vallecchi, M. Albani and F. Capolino, *Opt. Express*, 2013, **21**, 7667.
32 C. F. Bohren and D. R. Huffman, *Absorption and Scattering of Light by Small Particles*, Wiley-Interscience, New York, 1983.
33 T. Koschny, P. Markos, D. R. Smith and C. M. Soukoulis, *Phys. Rev. E: Stat., Nonlinear, Soft Matter Phys.*, 2003, **68**, 065602(R).
34 C. A. Dirdal, T. Bondevik and J. Skaar, *Phys. Rev. B: Condens. Matter Mater. Phys.*, 2015, **91**, 134102.
35 J. F. Schenck, *Med. Phys.*, 1996, **23**, 815.
36 D. C. Montgomery and G. C. Runger, *Applied statistics and probability for engineers*, J. Wiley & Sons, New York, 2010.
37 D. R. Smith, D. C. Vier, T. Koschny and C. M. Soukoulis, *Phys. Rev. E: Stat., Nonlinear, Soft Matter Phys.*, 2005, **71**, 036617.
38 V. G. Kravets, F. Schedin and A. N. Grigorenko, *Opt. Express*, 2010, **18**, 9780.